Formation of Ordered Nanoscale Semiconductor Dots by Ion Sputtering

S. Facsko,[1]* T. Dekorsy,[1] C. Koerdt,[1] C. Trappe,[1] H. Kurz,[1] A. Vogt,[2] H. L. Hartnagel[2]

A formation process for semiconductor quantum dots based on a surface instability induced by ion sputtering under normal incidence is presented. Crystalline dots 35 nanometers in diameter and arranged in a regular hexagonal lattice were produced on gallium antimonide surfaces. The formation mechanism relies on a natural self-organization mechanism that occurs during the erosion of surfaces, which is based on the interplay between roughening induced by ion sputtering and smoothing due to surface diffusion.

To date two approaches for the fabrication of semiconductor quantum dots have been pursued. In the top-down approach, lithographic methods are used for direct patterning of quantum dots, whereas the bottom-up approach relies on self-organized processes. In contrast to serial electron-beam lithography, self-organization phenomena open the way for the formation of a regular array of quantum dots on large areas in a single technological process step. Self-organized semiconductor quantum dots have been produced by the Stranski-Krastanow growth mode in molecular beam epitaxy and metal-organic vapor phase epitaxy, in which coherent island formation occurs during the growth of lattice-mismatched semiconductors (*1*). Here we present a controlled and cost-effective method for the production of well-ordered quantum dots by ion bombardment of semiconductor surfaces (*2*) that is based on a self-organization mechanism induced by ion sputtering of solid surfaces, where the formation kinetics is determined by etching instead of growth.

There has been great effort to interpret the microscopic dynamics of surface roughness and pattern formation induced by ion sputtering in which the formation of coherent ripples has been observed on metal, semiconductor, and insulator surfaces under ion bombardment at off-normal angles of incidence (*3–7*). The characteristic period in the submicrometer to nanometer range is defined by the sputtering conditions (for example ion energy, ion flux, and substrate temperature) and by the material properties. An explanation of the underlying mechanism was proposed by Bradley and Harper (*8*) in which the sputtering yield, which is the num-

ber of surface atoms removed per incident ion, depends on the surface curvature. Under certain conditions this dependence gives rise to a surface instability where the erosion is greater in a depression than on an elevation. The ion-induced surface instability can be described by a specific term in the erosion equation that is proportional to the negative Laplacian of the surface. The proportionality factor is called negative surface tension because it tends to maximize the surface, in contrast to surface tension that minimizes the surface. It is the competition between this roughening instability and diffusive smoothing mechanisms that governs the buildup of a regular pattern with a characteristic wavelength. Under off-normal incident ions the instability is anisotropic, giving rise to characteristic ripple patterns. Their direction was found to be either parallel or perpendicular to the direction of the ion beam depending on the angle of incidence. Generalized theories including also nonlinear terms and additional smoothing mechanisms, such as viscous flow on amorphous surfaces, have been developed (*4, 9, 10*). These theories allow the derivation of scaling laws that describe the roughening of ion-bombarded surfaces. Under normal incidence of the ion beam the surface morphology is expected to be a regular matrix of hillocks and depressions with a characteristic spatial frequency (*6*). However, these predictions could not be confirmed experimentally. We report here the experimental data showing that under normal incident Ar$^+$ ion sputtering highly ordered, densely packed nanostructures are induced on the surfaces of antimonides.

Low-energy Ar$^+$ ions were used in a commercial ion-sputtering system. The typical ion flux in the experiments was 1×10^{16} cm^{-2} s^{-1}. Under off-normal ion bombardment with 420-eV ion energy, coherent ripples were formed on GaSb surfaces with a period of 35 nm, in agreement with experimental observations reported for other materials (*3, 4, 6, 11, 12*). Under normal incidence, a highly regular pattern of dots appeared whose specific size and

shape depended on the ion fluence. The observations on dot formation were confirmed in experiments performed in a second commercial system with Ar atoms at the same energy and fluence as primary particles for sputtering.

Scanning electron microscope (SEM) images of a dot pattern induced on a (100) GaSb surface by 420-eV Ar$^+$ ions are shown for different ion fluences (Fig. 1, A to C) and the size distributions derived from the SEM images displayed (Fig. 1D). The evolution of dot formation can be traced from these data. At an ion fluence of 4×10^{17} cm^{-2}, equivalent to an exposure time, of 40 s, small dots with an average diameter of 18 nm [full width at half maximum (FWHM) 4 nm] appear. Their hexagonal ordering is already present, although some irregularities occur, and the dot density is 4.5×10^{10} cm^{-2}. After an exposure time of 200 s (fluence of 2×10^{18} cm^{-2}), the dot diameter has grown to 34 nm (FWHM 8 nm). The hexagonal ordering is clearly visible (Fig. 1B), and the dot density has slightly decreased because some of the earlier irregularities did not survive. Finally, after 400 s of exposure time, the average dot diameter is 50 nm (FWHM 6 nm) (Fig. 1C). The dot diameter approximately equals the period, and the hexagonal order is fully developed and represents the final stage of the dot formation. For longer exposure times the pattern does not change further, and the surface front propagates into the material with a constant velocity of 1.5 nm s^{-1} as the sample is eroded by the ion bombardment. This steady state was observed up to exposure times of 2 hours. The propagation of this strongly corrugated surface during depth profiling inhibited a good depth resolution of semiconductor heterostructures with secondary ion mass spectrometry.

The regular order of the dots is revealed by the two-dimensional (2D) autocorrelation pattern of a SEM image (Fig. 2). The autocorrelation pattern exhibits a nearly perfect hexagonal structure with a characteristic length of 45 nm over more than six periods, demonstrating that in addition to the self-assembly of the nanostructures a self-ordering process with a specific spatial frequency is operative.

A cross-sectional high-resolution transmission electron microscope (HTEM) image of the nanostructures produced by an ion exposure of 4×10^{18} cm^{-2} (same as in Fig. 1C) (Fig. 3) shows that the nanostructures have a cone-like shape with a sidewall angle of 60° to 70°. The cones are clearly crystalline with the same orientation and crystalline structure as the GaSb substrate. The high degree of crystallinity is observed within the whole cone, which is covered by an amorphous boundary ~2 nm thick that reveals a small perturbation of the crystal by the low-energy ions. Energy-dispersive x-ray spectrometry analysis on single cones confirmed

[1]Institute of Semiconductor Electronics, Rheinisch-Westfälische Technische Hochschule Aachen, Sommerfeldstrasse 24, 52074 Aachen, Germany. [2]Institut für Hochfrequenztechnik, TU Darmstadt, Merckstrasse 25, 64283 Darmstadt, Germany.

*To whom correspondence should be addressed. E-mail: facsko@iht-ii.rwth-aachen.de

that the stoichiometry is that of bulk GaSb.

Our data confirm the following picture. In the first seconds of the sputtering process a primary irregular roughness of the surface is induced by the stochastic nature of the ion bombardment (10, 13), by the preferential sputtering of Sb, and by the associated accumulation of Ga atoms on the surface. The amplification of the random amplitudes by the negative surface tension competes with processes such as surface diffusion and viscous flow that smooth the surface (8). Under certain conditions (10) these processes lead to the formation of a regular surface pattern by the exponential growth of a characteristic wavelength $\lambda \propto \sqrt{D/|v|}$, where D is a positive constant related to the surface diffusivity (14) and $|v|$ the largest absolute value of the negative surface tension coefficient (8, 15). The surface diffusion can be thermally activated or induced by ion bombard-

ment. Observation of dot formation with nearly the same period at sample temperatures of 60°C and −60°C reveals that, for the (100) GaSb surface, the ion-induced surface diffusion dominates in this temperature range (12). Similar processes have been identified to be the relevant mechanism for the formation of coherent ripples during ion bombardment. Under normal incidence, no orientation is distinguished by the sputtering process. As a consequence, ripples with all possible orientations could, in principle, evolve. The most stable solution under these circumstances is the formation of a hexagonal packed arrangement of dots as observed in our experiments.

Nanodot formation by ion sputtering of epitaxial GaSb layers grown by molecular beam epitaxy on higher bandgap materials, ideally on AlSb, opens the way to generate isolated dots with a three-dimensional confinement. We pro-

duced GaSb quantum dots on AlSb by sputtering a 500-nm GaSb layer down to the interface. Etching back to the interface was accomplished with high accuracy by monitoring the appearance of Al atoms with a mass spectrometer during the propagation of the steady-state pattern. The dots exhibit the same regularity and size distribution as the dots produced on bulk GaSb. Comparison of the photoluminescence of the dots on AlSb to that of bulk GaSb measured at low temperature (Fig. 4) reveals a weak and broad peak in the spectrum of the GaSb dots blue-shifted by ~300 meV as compared with the GaSb band edge luminescence. We attribute the blue shift to the quantum confinement in the dots. A residual line at the photon energy of bulk GaSb at 0.8 eV stems from the edge of the sputtered region. We attribute the fine structure on the spectrally broad peak to noise and not to the photoluminescence from single dots. The dot spectrum shows a
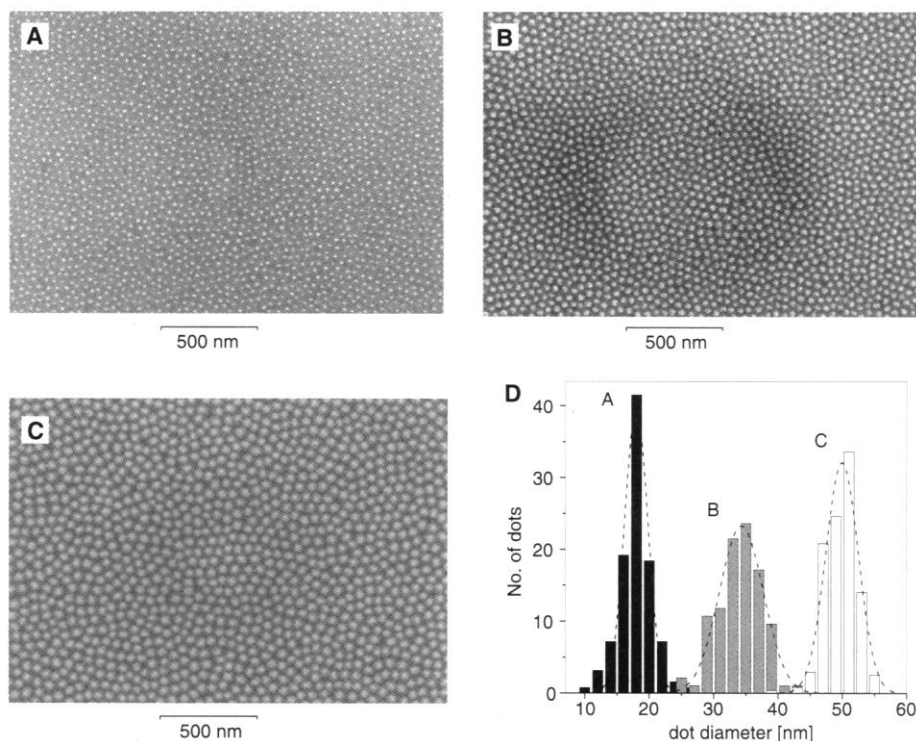

Fig. 1. SEM images of highly ordered cones on a (100) GaSb surface show the temporal evolution of dot formation during ion sputtering. The nanoscale patterns are depicted for different ion fluences (exposure times) of (**A**) 4×10^{17} cm^{-2} (40 s), (**B**) 2×10^{18} cm^{-2} (200 s), and (**C**) 4×10^{18} cm^{-2} (400 s). The corresponding size distributions of the dot diameters are extracted from the images (**D**). The dotted lines represent Gaussian fits to the dot diameter histograms.

Fig. 2. (**A**) The extract of a SEM image and (**B**) the corresponding two-dimensional autocorrelation reveal the regularity and hexagonal ordering of the dots, which extends over more than six periods.
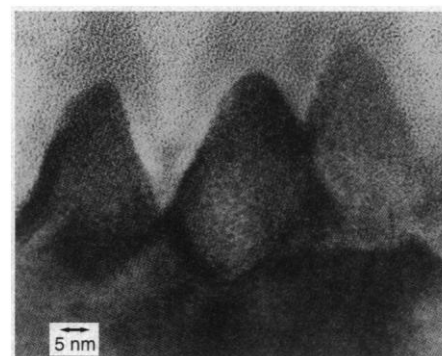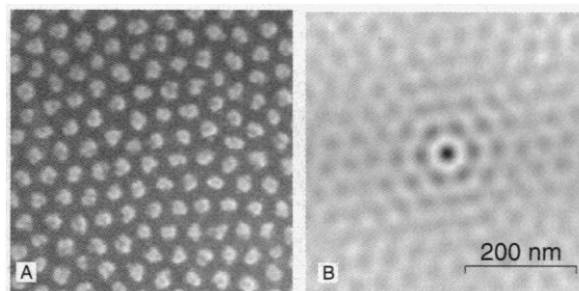

Fig. 3. Cross-sectional transmission electron microscope image of the nanostructures on a GaSb surface produced with the same parameters as in Fig. 1C. The dots are crystalline without a disruption to the crystal lattice of the GaSb bulk. An amorphous layer of ~2 nm, which is the penetration depth of the low-energy ions into the material, covers the dots. The base and the height of the dots measure 30 nm.
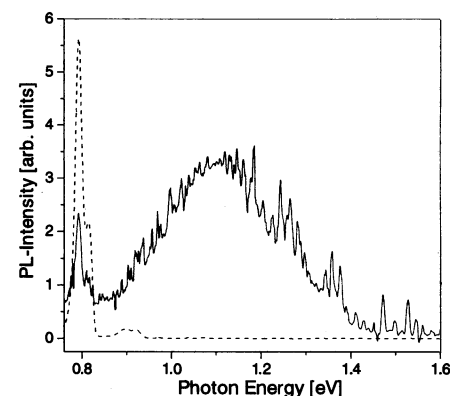

Fig. 4. The low-temperature (15 K) photoluminescence spectrum (in arbitrary units) of GaSb dots on an AlSb substrate shows a broad, weak spectrum. The solid line is the photoluminescence (PL) of the dots scaled up by a factor of 50 relative to the GaSb bulk spectrum, which is drawn as a dashed line.

large broadening (FWHM 290 meV) to which the inhomogenous distribution of the dot sizes strongly contributes ($\sim$170 meV). Additionally, the luminescence is expected to be broadened by electronic states as a result of a high density of ion-induced surface defects of these uncovered dots, seen in the HTEM image (Fig. 3) as a $\sim$2-nm-thick amorphous layer.

With respect to the potential of this technique for device fabrication, ion-induced defects have to be considered. These defects are sources for nonradiative recombination and therefore strongly deteriorate the optical and electrical properties. They must be reduced before devices can be fabricated. Possible methods are chemical etching, annealing, surface passivation, and overgrowth of the dots, methods which are performed ideally in situ. Overgrowth of the dots appears feasible because they exhibit a thermal stability up to 450°C.

The demonstration of regular dot formation on GaSb surfaces presented here may lay ground to extend the theory for ripple formation to normal incident ion sputtering. The formation mechanism for the nanometer-scaled dots relies only on the sputtering process and the diffusive transport on surfaces; therefore, we conclude that this mechanism should be universal and transferable to other materials. This conclusion is supported by experiments on InSb and Ge where the same dot formation as reported here for GaSb was observed (16). The successful demonstration of dot formation on Ge may open the way to produce nanostructures on the technologically important group IV semiconductor materials. The technical application of the produced nanostructures could include quantum dots for quantum devices and for black surfaces for optoelectronic and photovoltaic applications.

References and Notes
1. G. Springholz, V. Holy, M. Pinczolits, G. Bauer, *Science* **282**, 734 (1998); E. R. Glaser, B. R. Bennett, B. V. Shanabrook, R. Magno, *Appl. Phys. Lett.* **68**, 3614 (1996); M. Grundmann *et al.*, *Phys. Rev. Lett.* **74**, 4043 (1995).
2. S. Facsko *et al.*, patent pending.
3. G. Carter, B. Navinšek, L. Whitton, in *Sputtering by Particle Bombardment II*, vol. 64 of *Topics in Applied Physics*, R. Behrisch, Ed. (Springer-Verlag, New York, 1991), pp. 231–269.
4. E. Chason *et al.*, *Phys. Rev. Lett.* **72**, 3040 (1994).
5. T. M. Mayer, E. Chason, A. J. Howard, *J. Appl. Phys.* **76**, 1633 (1994).
6. G. Carter and V. Vishnyakov, *Phys. Rev. B* **54**, 17647 (1996).
7. S. Rusponi, C. Boragno, U. Valbusa, *Phys. Rev. Lett.* **78**, 2795 (1997); S. Rusponi, G. Constantini, C. Boragno, U. Valbusa, *ibid.* **81**, 4184 (1998).
8. R. M. Bradley and J. M. E. Harper, *J. Vac. Sci. Technol. A* **6**, 2390 (1988).
9. G. S. Bales *et al.*, *Science* **249**, 264 (1990).
10. R. Cuerno and A.-L. Barabási, *Phys. Rev. Lett.* **74**, 4746 (1995); R. Cuerno *et al.*, *ibid.* **75**, 4464 (1995).
11. M. Navez, C. Sella, D. Chaperot, *C. R. Acad. Sci.* **254**, 240 (1962).
12. S. W. MacLaren, J. E. Baker, N. L. Finnegan, C. M. Loxton, *J. Vac. Sci. Technol. A* **10**, 468 (1992).
13. G. Carter, M. J. Nobes, H. Stoere, I. V. Katardjiev, *Surf. Interface Anal.* **20**, 90 (1993).
14. The constant $D = D_s \gamma \Omega^2 n/k_B T$, where D_s is the surface diffusion constant, Ω the atomic volume, ν the area density of diffusing surface atoms, γ the surface free energy, k_B the Boltzmann constant, and T the temperature (8).
15. I. Koponen, M. Hautala, O.-P. Sievänen, *Phys. Rev. Lett.* **78**, 2612 (1997).
16. Regular dots with a diameter of 50 nm are observed on InSb(100) surfaces after an exposure time of 100 s to Ar$^+$ ions with an energy of 450 eV. On Ge(111) surfaces dots with a diameter of 16 nm could be observed after an Ar$^+$ ion exposure time of 1000 s with an ion energy of 1000 eV.
17. We thank D. Meertens and M. Feuerbacher (Institut für Festkörpesforschung, Forschungszentrum Jülich, Germany) for the HTEM images and the energy-dispersive x-ray spectrometry analysis and C. Moormann (Advanced Microelectronic Center Aachen, Aachen, Germany) for the SEM pictures.

17 March 1999; accepted 9 July 1999

KDR Receptor: A Key Marker Defining Hematopoietic Stem Cells

B. L. Ziegler,*[1] M. Valtieri,*[2,3] G. Almeida Porada,[4] R. De Maria,[2,3] R. Müller,[1] B. Masella,[2] M. Gabbianelli,[3] I. Casella,[2] E. Pelosi,[3] T. Bock,[1] E. D. Zanjani,[4] C. Peschle[2,3]†

Studies on pluripotent hematopoietic stem cells (HSCs) have been hindered by lack of a positive marker, comparable to the CD34 marker of hematopoietic progenitor cells (HPCs). In human postnatal hematopoietic tissues, 0.1 to 0.5% of CD34$^+$ cells expressed vascular endothelial growth factor receptor 2 (VEGFR2, also known as KDR). Pluripotent HSCs were restricted to the CD34$^+$KDR$^+$ cell fraction. Conversely, lineage-committed HPCs were in the CD34$^+$KDR$^-$ subset. On the basis of limiting dilution analysis, the HSC frequency in the CD34$^+$KDR$^+$ fraction was 20 percent in bone marrow (BM) by mouse xenograft assay and 25 to 42 percent in BM, peripheral blood, and cord blood by 12-week long-term culture (LTC) assay. The latter values rose to 53 to 63 percent in LTC supplemented with VEGF and to greater than 95 percent for the cell subfraction resistant to growth factor starvation. Thus, KDR is a positive functional marker defining stem cells and distinguishing them from progenitors.

The hierarchy of human hematolymphopoietic cells is defined by functional assays. HSCs with extensive self-renewal capacity are assayed in vivo for their capacity to xenograft nonobese diabetic–severe combined immunodeficiency disease (NOD-SCID) mice and sheep fetuses (1–3). These models are surrogates for a syngeneic transplantation assay. Primitive HPCs with limited self-renewal potential are identified in vitro as high–proliferative potential colony-forming cells (HPP-CFCs) (4). Lineage-committed HPCs with no self-renewal activity are also defined in vitro by clonogenic assays as colony-forming units (CFUs) or burst-forming units (BFUs) (1, 5). Dexter-type LTC, consisting of a liquid phase on irradiated BM stroma, identifies LTC-initiating cells (LTC-ICs, gener-

ating HPCs assayed in secondary culture) (6) and cobblestone area–forming cells (CAFCs, generating hematopoietic colonies recognized as "cobblestone areas" in LTC stroma) (7). Depending on the LTC duration, LTC-ICs represent primitive HPCs (5- to 8-week LTC) (8) or highly quiescent putative HSCs resistant to retroviral gene transfer (12-week LTC) (9) (see below).

Although HSC identification is still elusive, recent observations have suggested a role for VEGFR2 (Flk1 in mice) in murine embryonic hematoangiogenesis. Targeted gene disruption studies indicate that Flk1 is required for initiation of hematolymphopoiesis and vasculogenesis (10), implying that Flk1 may be required for generation of hemoangioblasts, that is, the hypothetical stem cells for both hematolymphopoietic and endothelial lineages (11). Other studies also suggested the existence of embryonic Flk1$^+$ cells with hemoangiogenic potential but did not allow identification of prenatal repopulating HSCs (12). We identified KDR as a major functional marker for postnatal HSCs.

In postnatal life, KDR is expressed on endothelial cells (13), and the mRNA can be detected in HPCs and megakaryocytes (14, 15). We used a high-affinity monoclonal antibody (mAb clone 260.4) that binds the extracellular

[1]Department of Hematology and Oncology, University of Tübingen, Otfried-Müller-Strasse 10, D-72076 Tübingen, Germany. [2]Kimmel Cancer Institute, Thomas Jefferson University, 233 South 10 Street, Philadelphia, PA 19107–5541, USA. [3]Department of Hematology and Oncology, Istituto Superiore di Sanità, V. le Regina Elena 299, 00161 Rome, Italy. [4]Department of Veterans Affairs, University of Nevada, Reno, NV 89520, USA.

*These authors contributed equally to this work.
†To whom correspondence should be addressed. E-mail: cesare.peschle@mail.tju.edu